



Dynamic Stall Prediction of a Pitching Airfoil using an Adjusted Two-Equation URANS Turbulence Model

G. Bangga^{1,2†} and H. Sasongko²

¹ *Institute of Aerodynamics and Gas Dynamics, University of Stuttgart, Germany*

² *Mechanical Engineering Department, Institut Teknologi Sepuluh Nopember, Indonesia*

†Corresponding Author Email: bangga@iag.uni-stuttgart.de

(Received April 10, 2016; accepted August 24, 2016)

ABSTRACT

The necessity in the analysis of dynamic stall becomes increasingly important due to its impact on many streamlined structures such as helicopter and wind turbine rotor blades. The present paper provides Computational Fluid Dynamics (CFD) predictions of a pitching NACA 0012 airfoil at reduced frequency of 0.1 and at small Reynolds number value of $1.35e5$. The simulations were carried out by adjusting the $k - \epsilon$ URANS turbulence model in order to damp the turbulence production in the near wall region. The damping factor was introduced as a function of wall distance in the buffer zone region. Parametric studies on the involving variables were conducted and the effect on the prediction capability was shown. The results were compared with available experimental data and CFD simulations using some selected two-equation turbulence models. An improvement of the lift coefficient prediction was shown even though the results still roughly mimic the experimental data. The flow development under the dynamic stall onset was investigated with regards to the effect of the leading and trailing edge vortices. Furthermore, the characteristics of the flow at several chords length downstream the airfoil were evaluated.

Keywords: Computational fluid dynamics; Flow turbulence; Pitching airfoil; Vortex flow.

NOMENCLATURE

c	chord length	x, y, z	cartesian coordinates
C_b	damping factor according to realizable $k - \epsilon$	y^+	non-dimensional wall distance
C_l	model lift coefficient	Y_k	dissipation term for k
f	damping factor as a step function	Y_ϵ	dissipation term for ϵ
f_b	damping factor	α	angle of attack
G_k	production term for k	α_0	mean angle of attack
G_ϵ	production term for ϵ	δ_{ij}	kroncker delta
k	turbulent kinetic energy	$\Delta\alpha$	oscillation amplitude
l	turbulent length scale	ϵ	energy dissipation
Re_c	Reynolds number based on the chord length	μ	laminar viscosity
S	mean rate-of-strain tensor	μ_t	eddy viscosity
S_k	user defined source for k	ρ	density
S_ϵ	user defined source for ϵ	σ_k	turbulent Prandtl number for k
TI	turbulent intensity	σ_ϵ	turbulent Prandtl number for ϵ
$u_{i,j,k}$	x, y, z velocities	\emptyset	phase angle
$u'_{i,j,k}$	fluctuating x, y, z velocities	$\hat{\omega}_k$	reduced frequency, $\omega_k c / 2V$
V	free stream velocity	ω_k	angular velocity

1. INTRODUCTION

The aerodynamic loads of helicopter and wind turbine rotors have a strong time dependency

toward periodic changes of the angle of attack as the results of input angles, blade flapping, yaw misalignment, shear flow, and blade-wake interaction which lead to dynamic stall. The onset

of dynamic stall is characterized by the formation of an intense vortical structure near the leading edge of the sectional airfoil causing the lift coefficient (C_l) to increase beyond the static stall angle widely known as stall delay. This vortical structure is convected on the suction side of the airfoil indicated by the lift gradient increase. At a certain value of α near $C_{l,max}$, the vortex detaches from the airfoil body and starts to breaking down followed by the formation of the trailing edge vortex. This behavior is marked by a significant drop in C_l . The aerodynamic loads received by the structures usually is far greater than in the static condition, increasing the stress field of the blade support system and has a huge potential to harm the structure itself (Witteveen *et al.* 2007).

Understanding the dynamic stall behaviour is important for accurate prediction of the aerodynamic loading on rotating machineries (Johansen 1999). Many studies have been conducted to reveal the dynamic stall mechanism (Bangga and Sasongko 2012; Naderi *et al.* 2016). Until the middle of 20th century, the dynamic stall was only studied experimentally due to limitation of the background data to govern the mathematical formulations. In the late of 1970s, Friedmann (Friedmann 1983) described three models and, afterwards, mathematical modelling on dynamic stall was developing (Hansen *et al.* 2004). The models ranged from simple to complex such as ONERA (Petot 1989), Boeing (Friedmann 1983), Johnson (Johnson and Ham 1972; McCroskey *et al.* 1976), Øye (Øye 1991), Risø (Hansen *et al.* 2004) and also Leishman-Beddoes models (Leishman and Beddoes 1989; Hansen *et al.* 2004).

With the advent of computer performance, Computational Fluid Dynamics (CFD) simulations of the dynamic stall became possible. At the beginning, the compressibility effect was neglected due to limitation of the computational time (Fung and Carr 1991). This problem was brought up again to the surface in the late of '90s by considering the compressibility and turbulence model influences (Ekaterinaris 1995; Ekaterinaris *et al.* 1995; Barakos and Drikakis 2003). However, due to the lack of robust CFD methods, most CFD works were done only focusing on the validation of the CFD codes rather than the physical phenomena of the flow. Wang *et al.* (Wang *et al.* 2010; Wang *et al.* 2012) demonstrated that the Shear-Stress-Transport (SST) $k - \omega$ turbulence model gave better prediction compared to the Wilcox $k - \omega$ for 2D case, but the predicted aerodynamic polar was rather non-smooth with a strong non-physical fluctuation along the whole range of α . Belkheir *et al.* (Belkheir *et al.* 2012) performed 2D and 3D CFD calculations of an airfoil using $k - \epsilon$ and SST $k - \omega$ models. The SST model gave a better prediction but the lift was overestimated and a strong fluctuation of the lift was observed in the down-stroke phase. Szydłowski and Costes (Szydłowski and Costes 2004) showed the prediction of static and oscillating airfoils using Unsteady Reynolds-Averaged Navier-Stokes (URANS), Detached Eddy Simulations (DES) and Large Eddy Simulations

(LES) models. The LES model clearly showed the superiority while the URANS and DES were struggling in predicting the laminar to turbulent transition, but the computational cost increased considerably in LES simulations.

Past studies on turbulent flow have shown that the accuracy of numerical predictions is significantly affected by the accuracy of the employed turbulence model (Barakos and Drikakis 2003). The zero-equation turbulence model was shown to inaccurately predict separated flow by Baldwin and Lo-max (Baldwin and Lomax 1978). The linear eddy-viscosity models have several advantages in the prediction for turbulent flows. They provide satisfactory results for attached, fully developed turbulent boundary layers with weak pressure gradients and are also relatively easy to implement into CFD codes (Barakos and Drikakis 2003). Among them, two-equation eddy viscosity turbulence models were the most commonly used in practice.

It has been agreed that it was too naive and dangerous to assume the validity of a turbulence model in the wide range of flows (Arabshahi *et al.* 1998). It has been commonly known that the URANS models were inaccurate to predict the flow past airfoils beyond stall and often over predicted the maximum lift coefficient (Shur *et al.* 1999; Szydłowski and Costes 2004). Chitsomboon and Thamthae (Chitsomboon and Thamthae 2011) has shown that the overestimation came from the excessive turbulence level within the boundary layer, enhancing the momentum transfers to the near wall regions which helps the boundary layer to push through the adverse pressure gradient regions.

The objective of the present study is to improve the prediction of the dynamic stall through an adjusted two-equation URANS turbulence model. The turbulence production is damped through the introduction of a damping function in the buffer zone. The $k - \epsilon$ turbulence model was chosen as the base because it is one of the most commonly used turbulence models in industry and its simplicity makes the implementation of the damping factor easier. Parametric studies are conducted to observe the impact of the individual parameter implemented in the model. The study of the dynamic stall mechanism is conducted through an observation of the dynamic stall vortices. Finally, the wake flow pattern under dynamic motion of the airfoil is evaluated.

The paper is organized as follows. The test case and numerical procedures are given in section 2. Section 3 presents the results, and the conclusion is made in section 4.

2. COMPUTATIONAL APPROACHES

2.1 Adjustment of the Turbulence Model

In this section, the governing equations of the adjusted turbulence model are given. The $k - \epsilon$ URANS turbulence model is one of the most common model used in computational fluid

dynamics regarding the simulation of the mean flow characteristics for turbulent flow conditions. The model is governed by two transport equations, one for turbulent kinetic energy and one for its dissipation rate. The original model was proposed by Launder and Spalding (Launder and Spalding 1972) and has become the workhorse of practical engineering flow calculations in the time since then. The original $k - \varepsilon$ or “standard” $k - \varepsilon$ turbulence model is a semi-empirical model combined the exact equation for k and non-exact formulation for ε . The equation for dissipation rate was governed using physical reasoning and bears little resemblance to its mathematically exact counterpart. The transport equations for k and ε are given in Eqs. (1) and (2), respectively.

$$\frac{\partial}{\partial t}(\rho k) + \frac{\partial}{\partial x_i}(\rho k u_i) = \frac{\partial}{\partial x_j} \left[\left(\mu + \frac{\mu_t}{\sigma_k} \right) \frac{\partial k}{\partial x_j} \right] + G_k - \rho \varepsilon + S_k \quad (1)$$

$$\frac{\partial}{\partial t}(\rho \varepsilon) + \frac{\partial}{\partial x_i}(\rho \varepsilon u_i) = \frac{\partial}{\partial x_j} \left[\left(\mu + \frac{\mu_t}{\sigma_\varepsilon} \right) \frac{\partial \varepsilon}{\partial x_j} \right] + C_{1\varepsilon} \frac{\varepsilon}{k} G_k - C_{2\varepsilon} \frac{\varepsilon^2}{k} + S_\varepsilon \quad (2)$$

In these equations, G_k represents the generation of turbulence kinetic energy due to the mean velocity gradients, approximated in a consistent manner using oussinesq assumption, $G_k = \mu_t S^2$. S is defined as $\sqrt{2S_i j S_i j}$. The turbulent viscosity is defined as

$$\mu_t = f_b \rho C_\mu \frac{k^2}{\varepsilon} \quad (3)$$

with C_μ is a constant with the value of 0.99. The other constants value are $C_{1\varepsilon} = 1.44$, $C_{2\varepsilon} = 1.92$, $\sigma_\varepsilon = 1.0$, $\sigma_k = 1.3$.

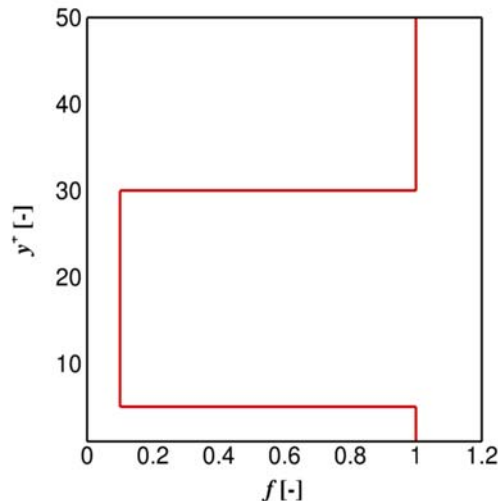


Fig. 1. Damping as a step function for the case of $f = 0.1$.

The only difference of the present modification with the original $k - \varepsilon$ model is the addition of variable f_b in Eq. (3). This parameter is defined as

$$f_b = f C_b \quad (4)$$

The parameter f is adopted from the near wall treatment according to Chitsomboon and Thamthae (Chitsomboon and Thamthae 2011) using step function, Fig. 1. The value of f is damped on the buffer zone around $5 < y^+ < 30$ and is unity on the other zones.

Based on the knowledge on several turbulence models, realizable $k - \varepsilon$ model (Shih *et al.* 1995) is likely perform better than the standard $k - \varepsilon$ model in many aspects such as flows involving rotation, boundary layers under strong adverse pressure gradients, separation, and recirculation. Hence, we made use of this advantages and applied the damping factor, C_b , according to this model. It is defined as

$$C_b = \frac{1000}{A_0 + A_1 \frac{k U^*}{\varepsilon}} \quad (5)$$

With

$$U^* = \sqrt{S_{ij} S_{ij} + \tilde{\Omega}_{ij} \tilde{\Omega}_{ij}} \quad (6)$$

$$\tilde{\Omega}_{ij} = S_{ij} - 2 \varepsilon_{ijk} w_k \quad (7)$$

$$S_{ij} = \frac{1}{2} \left(\frac{\partial u_j}{\partial x_i} + \frac{\partial u_i}{\partial x_j} \right) \quad (8)$$

The constants A_0 and A_1 have the values of 4.04 and $\sqrt{6}$, respectively.

2.2 Test Case and Computational Mesh

This section provides the description of the numerical schemes used of the studied case. The commercial software package ANSYS Fluent 13.0 was used in this computation. Two dimensional analysis was selected because it is quite useful for observation of the flow characteristics and it can be useful in predicting the aerodynamic dependency of various parameters (Naderi *et al.* 2016). The SIMPLE algorithm was applied in the pressure velocity coupling and all equations to obtain a simultaneous solution (Wang *et al.* 2010). First order discretization for the momentum equations was used. It should be noted that the primary goal of this study is not to mimic the experiment results, but to demonstrate the improvement of the CFD predictions using the present modification. For the purpose of accurate simulations, the use of higher order schemes or even WENO scheme (Shu 2003) is strongly recommended. In this study, apart from the adjusted model, four other well-known turbulence models were used for comparison, namely standard $k - \varepsilon$, realizable $k - \varepsilon$, Wilcox $k - \omega$ and SST $k - \omega$. The standard wall function was used for all $k - \varepsilon$ based turbulence models.

The harmonically pitching NACA 0012 airfoil at a reduced frequency of $\omega_k = 0.1$ was chosen as a test case. The center of rotation was located on the leading edge. The mean angle of attack was chosen equal to 10° and the amplitude was set to 15° . The

airfoil was operating at the chord based Reynolds number of $1.35e5$ with the chord length of $c = 0.15m$. The velocity, turbulent intensity and turbulent length scale at the inlet boundary was set equal to $14m/s$, 0.08% and $0.0001m$, respectively. The turbulent length scale near the airfoil can be approximated as $l \sim cRe^{-1/5}$. The timestep was then calculated as $\Delta t = 2\pi l/V$ so that the timestep value is small enough to resolve the small eddies close to the airfoil.

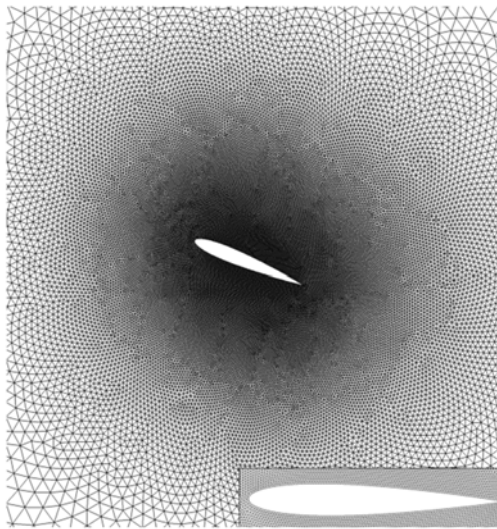


Fig. 2. The mesh used in the calculations.

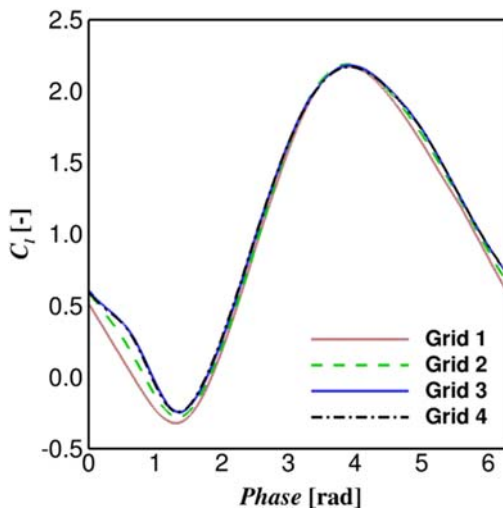


Fig. 3. Grid independency study. Airfoil grid points: Grid 1, 80 points; Grid 2, 120 points; Grid 3, 204 points; Grid 4, 215 points.

The mesh was built using unstructured triangular mesh to accommodate the movement of the airfoil. It was modelled using the dynamic mesh approach with rigid body motion. Spring based smoothing scheme was adopted with the constant equal to zero, indicating zero damping value on the airfoil surface. The remeshing method was set on the local cells with the minimum length scale of $0m$, maximum length scale of $0.8m$, minimum cell skewness of 0.4

and size remeshing interval of unity. The number of grid points on the suction and pressure sides of the airfoil was 204. The mesh can be seen in Fig. 2. The inlet and the outlet boundaries were set as velocity inlet and pressure outlet boundary conditions, respectively, while the side wall boundary and the airfoil surface were non-slip walls. The grid studies were conducted using the standard $k - \epsilon$ turbulence model and the results are plotted in Fig. 3. Grid 3 was chosen and used for all simulations presented in this paper.

3. RESULTS AND DISCUSSION

3.1 Parametric Study

In this section, parametric study on the damping effects are given. The modification involves two main parameters, f and C_b , which give an impact on the prediction of the flow under dynamic stall for low Reynolds number. Fig. 4 shows the effect of the damping parameter f on the lift coefficient value at different phase angles. In these results, C_b was switched off ($C_b = 1.0$) for the isolation purpose. It can be seen that that the parameter has a strong impact on the predicted lift from the phase angles (ϕ) 0 to 5 radians. With decreasing damping value, f , the lift coefficient increases significantly at $0 < \phi < 2$ and reduces at $2 < \phi < 5$.

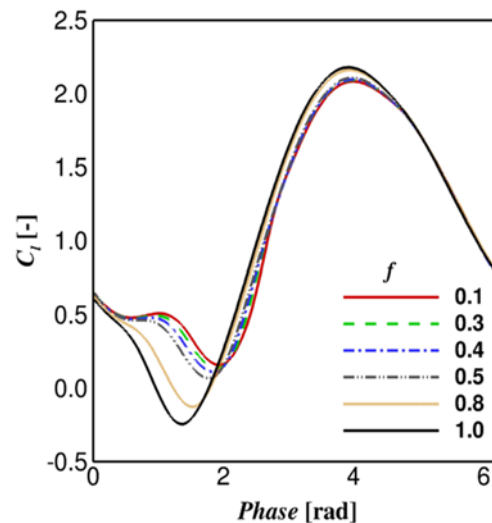


Fig. 4. Parametric study of variable f . It shall be noted that $f = 1.0$ represents no damping condition.

The increasing lift phase is the region where the airfoil changes its motion from downstroke to upstroke, see Fig. 5. It should be noted that the zero phase angle is equal to $\alpha = 10^\circ$ after fully developed flow is reached in the simulations. This behaviour is driven by the convecting vortex on the suction side of the airfoil. A lower damping value tends to influence the leading edge vortex strength and to increase the velocity field near the suction side. On the other hand, higher pressure value is predicted on the pressure side and this contributes to lift increase in Fig. 4.

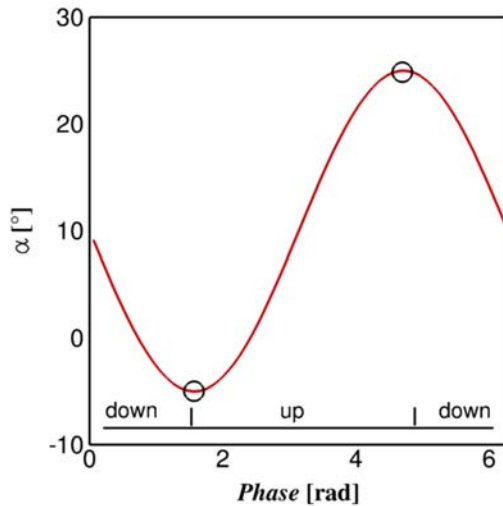


Fig. 5. Relation between phase angle and α .

The introduction of parameter C_b gives a counter-balance of the results for the parameter f . Fig. 6 shows the effect of the parameter C_b on the lift prediction of an oscillating airfoil. It can be seen that the lift coefficient decreases at $0 < \varphi < 2$. The cause of this reduction is the inclusion of rotation parameter in the governing equation in Section 2.1. Thus, the excessive momentum transfer of the flow over the suction side is alleviated, resulting in a smaller C_l value. On the other hand, C_l slightly increases at $2 < \varphi < 5$, but in a smaller order of magnitude than C_l reduction for parameter f . Hence, the effect should be small.

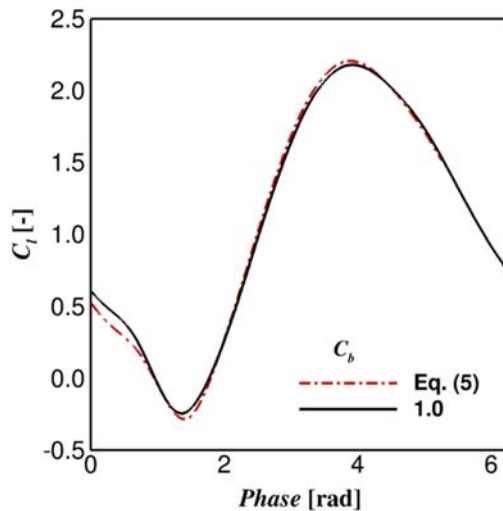


Fig. 6. Parametric study of variable C_b . It shall be noted that $C_b = 1.0$ represents no damping condition.

3.2 Performance of the Modified Model

This section provides the comparison of the proposed model to some selected two-equation URANS turbulence models and measurement data from Lee and Gerontakos (Lee and Gerontakos 2004). Based on the parametric study in Section 3.1,

the damping factor is constructed by combining parameters f and C_b . The value of $f = 0.3$ was chosen in this work. The chosen value is based on the observation of the parametric study in Fig. 4. There can be seen that the resulting C_l distributions are similar for $f = 0.1 - 0.5$. Thus, it is recommended to choose the parameter value within this range.

Figure 7a shows the comparison of the present model to the standard $k - \epsilon$ turbulence model. It can be seen that the introduction of the damping parameter improves the prediction of the lift polar. The overestimated C_l for the whole upstroke phase is reduced although the reduction is not that significant. However, there is an important characteristic of the oscillating airfoil which cannot be predicted using the standard model: the switch of the lift behaviour at small angles of attack which produces the bundle of C_l , the green circle dot in Fig. 7a. On the other hand, this behaviour can be predicted by the present model even though the location is not accurately estimated; $\alpha_{CFD} = -2.8^\circ$ and $\alpha_{Exp.} = 0^\circ$.

The prediction using the realizable $k - \epsilon$ model in Fig. 7b shows a similar result with the present model. This characteristic comes from the fact that C_b in the present model was governed by mimicking the turbulence viscosity equation in the realizable $k - \epsilon$ model (Shih *et al.* 1995). However, the addition of parameter f improves the prediction of the lift. There is a massive reduction of C_l in the downstroke phase which makes the results closer to the measurement data. Both models successfully predicted the bundle of lift, but at different angle and at different value.

Flows over a low Reynolds number value are the speciality of the $k - \omega$ based turbulence models (Wilcox *et al.* 1998). The models predict in a good agreement for many engineering applications involving shear flows (Hutomo *et al.* 2016; Bangga *et al.* 2015b; Bangga *et al.* 2015a). The predictions using these models are presented in Figs. 7c and 7d. Similar with the realizable $k - \epsilon$ model, the proposed model predicts very similar results with the Wilcox $k - \omega$ and SST $k - \omega$ turbulence models. The improvements are observed in the downstroke phase and all models can predict the lift bundle. It should be noted that the prediction of the bundle using the modified $k - \epsilon$ model is very similar with the SST model (Fig. 7d). The value is better predicted using the present model but the location is otherwise.

In the present simulations, all turbulence models fail to mimic the experimental data accurately. Several explanations can be given regarding this issue. The measurements were conducted on natural transition and no boundary layer tripping was applied, but the present simulations were conducted on the fully turbulent boundary layer without any transition prescription. This results in an excessive turbulence production since there is no laminar arc length on the airfoil surface. In consequence, the leading edge vortex has an enormous energy and this results in a higher lift value.

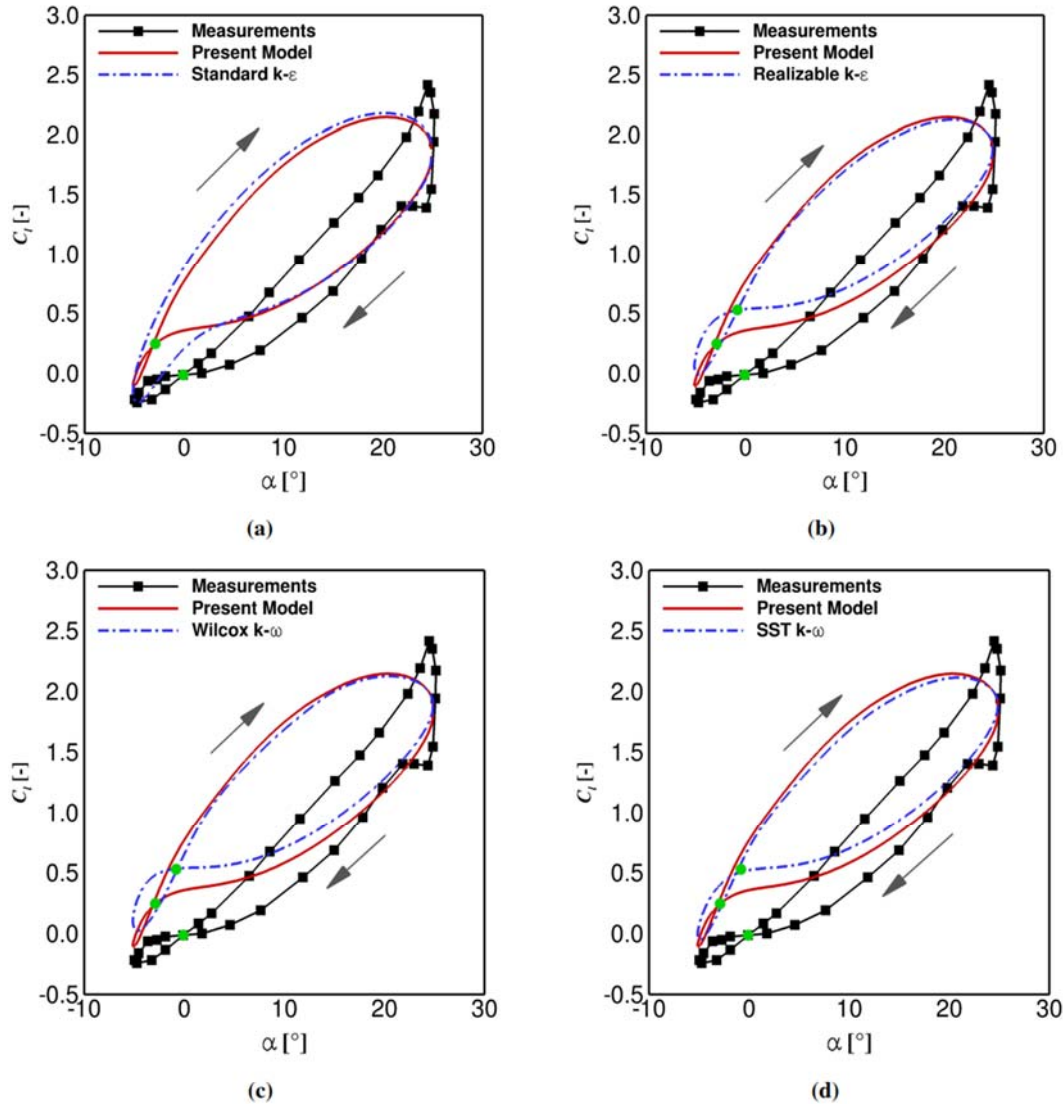


Fig. 7. Comparison of the present model to the other two-equation URANS models.

The other reasons are related to the numerical schemes and discretization. As mentioned in Section 2.2, the goal of the present work is not to accurately predict the forces but to demonstrate the improvement of the modification using a small order discretization for faster and simpler analyses. The effect of numerical discretization is presented in Fig. 8. It can be seen that discretization order shows strong impact on both turbulence models, standard and adjusted $k - \epsilon$. The impact is more pronounced around $0 < \varphi < 2.5$ and $4 < \varphi < 6$. Converged results with regard to the discretization order is shown for the 2nd order case. Therefore, it is recommended to use 2nd order discretization for future simulations.

3.3 Dynamic Stall Mechanism

To better understand the dynamic stall characteristics, this section provides the analyses of the vortical structures development under dynamic stall and their impact on the near wake region. Fig.

9 shows the plot of vorticity in the spanwise direction for different angles of attack during the full cycle of dynamic stall onset at low Reynolds number.

It can be seen clearly that a massive vortex is observed on the suction side of the airfoil at the smallest angle of attack, Fig. 9a. This vortex travels downstream and detaches from the airfoil body at higher angles of attack. The flow is then fully attached on the suction side as shown in Fig. 9c at $\alpha = 1^\circ$. However, the shedding vortices are still observed downstream the trailing edge. The lift coefficient increases up to $\alpha = 20.3^\circ$ as depicted in Fig. 9f. At this position, the strength of the vorticity field grows stronger near the leading edge, increasing the boundary layer thickness. Further increase of the angle of attack reduces slightly the lift coefficient and small flow separation is observed near the front side of the airfoil (Fig. 9g).

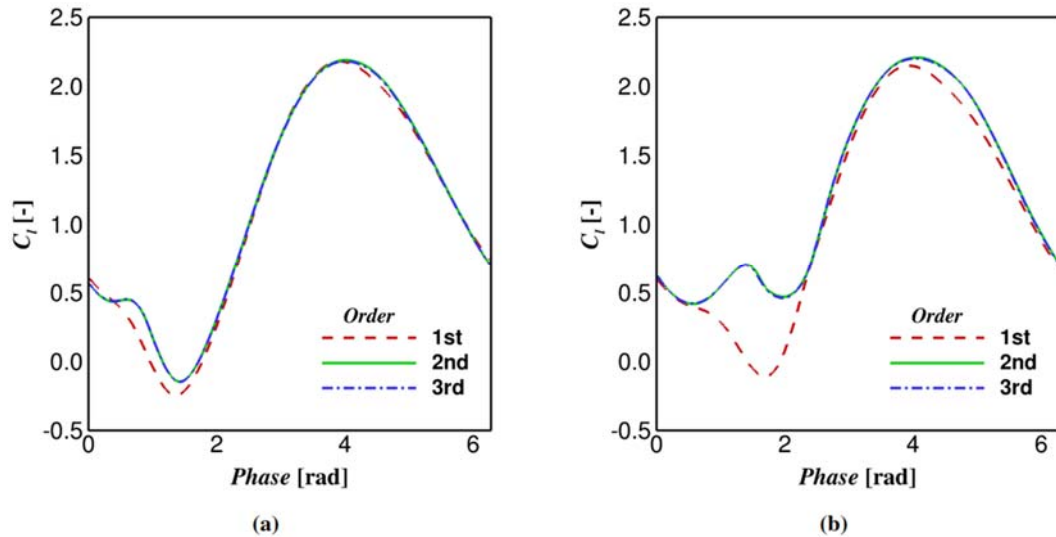


Fig. 8. Discretization order impact for (a) standard and (b) adjusted $k - \epsilon$ models.

Just right after the downstroke phase begins, the boundary layer thickness near the leading edge on the suction side grows rapidly, creating separation and reattachment mechanism which produces the leading edge vortex. This vortex travels downstream with decreasing α value, shown in Figs. 8h-8l, which preserves even until the end of the down-stroke phase. In consequence, the lift increases at small angle of attack in the downstroke phase. On the other hand, the breakdown of the leading edge vortex, observed in the upstroke phase at small α (Fig. 9a), contributes to the reduction of lift. This creates the bundle of lift polar observed in Fig. 7.

This characteristic is different with the general dynamic stall behaviour in which the shedding of the leading edge vortex occurs in the up-stroke phase. McCroskey *et al.* (McCroskey *et al.* 1976) explained this behaviour as the phase shift and it is strongly influenced by the reduced frequency. Bangga and Sasongko (Bangga and Sasongko 2012) performed CFD simulations of an oscillating rotocraft airfoil at a reduced frequency of 0.62. They observed an alternating domination of the leading edge and the trailing edge vortices at high angles of attack, resulting in the lift fluctuation. It is strongly different with the present study ($\omega k = 0.1$) which shows the domination of the fully attached flow for the upstroke phase, even at high angles of attack.

The phase shifting explained above is strongly influenced by the adverse pressure gradient and the location of the stagnation point which moves periodically with the change of the angle of attack. The stagnation location is shifted far downstream at high angle of attack, and this produces a very strong positive pressure gradient. In consequence, flow separation occurs on the leading edge. However, since the airfoil is fastly pitching, there is an additional circulation induced by the upstroke motion which makes the flow remains attached.

For instance see Fig. 8f where the flow is fully attached.

In addition to the phase shifting explained above, three observation points downstream of the airfoil were monitored during the simulations for the analysis of the near wake region. They are located at $0.25c$, $0.75c$ and $1.25c$ behind the airfoil. The extracted data are the instantaneous velocities in the x - and y -directions and the results are plotted in Fig. 10.

It can be seen that the velocity range during the cycle of the dynamic stall onset decreases with increasing chordwise distance from the trailing edge. For instance, the ranges for the observation point of $x/c = 0.25$ are $0.5 < u/V < 1.23$ and $-0.34 < v/V < 0.6$. They are reduced by 37% ($x/c = 0.75$) to 56% ($x/c = 1.25$) for x -velocity and 24% ($x/c = 0.75$) to 35% ($x/c = 1.25$) for y -velocity.

What interesting is that the upstroke motion occupies a longer velocity plot line than the downstroke motion, and the difference decreases with the downstream distance. It can be divided into four main categories, see Fig. 10. Zone (1)-(2) is where the leading edge vortex detaches from the airfoil body and interacts with the trailing edge vortex so that y -velocity increases (Fig. 9a). Zone (2)-(3) shows the typical velocity characteristic for a fully attached flow; x - and y -velocities decrease with α . Zone (3)-(4) is where the boundary layer thickness thickening starts and Zone (4)-(5) is where the leading edge vortex is formed.

The shape of the velocity plot is strongly influenced by the airfoil oscillation. A complicated pattern is observed in Fig. 10 and this is expected as the results of the phase shifting phenomenon due to high reduced frequency value. It confirms the conclusion made by Chen and Ho (Chen and Ho 1987) who demonstrated that the velocity field of an unsteady airfoil was affected by the reduced frequency, amplitude and angle of attack.

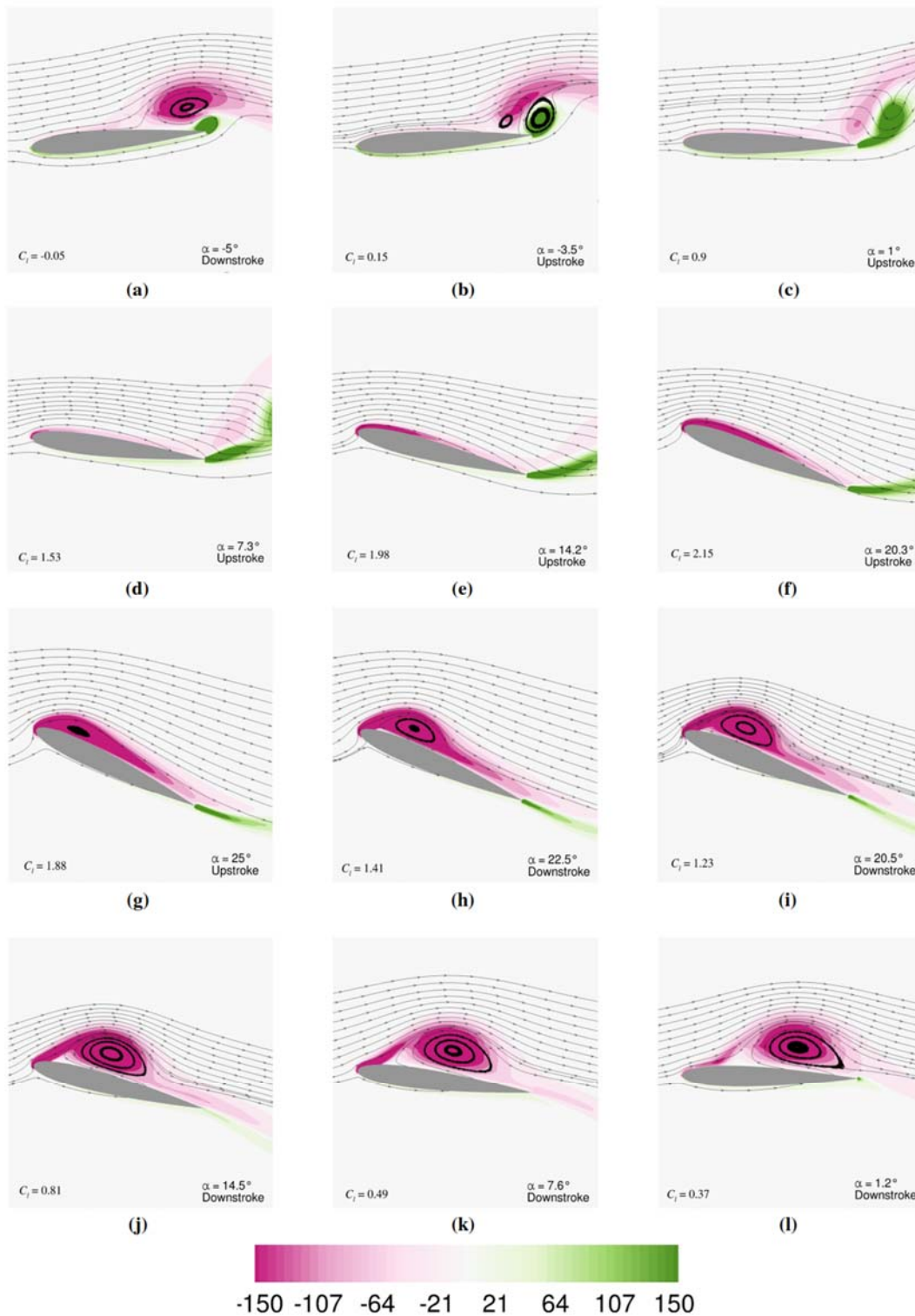


Fig. 9. Development of the leading edge vortex colored by spanwise vorticity value in [1/s].

4. CONCLUSION

In the present study, an oscillating airfoil has been simulated using an adjusted two-equation turbulence model. A damping factor was introduced and implemented in the standard $k - \varepsilon$ turbulence model. The proposed damping was governed based on the wall distance and a parameter which was

adopted from the realizable $k - \varepsilon$ model. The modification has an impact on the prediction of the lift coefficient over the airfoil. A better performance was demonstrated and compared with four selected two-equation URANS turbulence models even though the results are still far from the experimental data due to several reasons such as the transition location, numerical schemes, and mesh size.

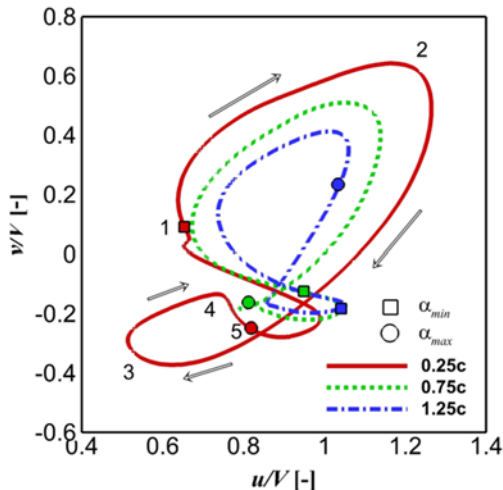


Fig. 10. Velocity plot in the near wake region.

The dynamic stall phenomenon studied in this work was observed through the observation of the vortex development. The leading and trailing edge vortices were captured in the present study. The phase shifting occurred and the convection of the leading edge vortex was observed in the downstroke phase. This phenomenon shows a strong impact on the near wake flow behind the airfoil. The velocity ranges of a point downstream the airfoil decrease with the distance from the specific point to the trailing edge, and this is highly influenced by the reduced frequency.

The present study accompanied only a specific case and it was calculated with the low order numerical schemes for faster and simpler analyses. It has been shown that numerical scheme order affected the force prediction. For future studies, it is suggested to use at least 2nd order schemes for accurate results. Furthermore, because the onset of dynamic stall is actually 3D effects, 3D CFD simulations are encouraged to be performed.

ACKNOWLEDGMENT

The authors would like to acknowledge the Ministry of Research, Technology and Higher Education of Indonesia for the financial support through DGHE scholarship.

REFERENCES

Arabshahi, A., M. Beddhu, W. Briley, J. Chen, A. Gaither, J. Janus, M. Jiang, D. Marcum, J. McGinley, R. Pankajakshan and *et al.* (1998). A perspective on naval hydrodynamic flow simulations. In *Proceeding of 22nd ONR Symposium on Naval Hydro* 920–934.

Baldwin, B. S. and H. Lomax (1978). Thin layer approximation and algebraic model for separated turbulent flows. *American Institute of Aeronautics and Astronautics* 257.

Bangga, G. and H. Sasongko (2012). Numerical investigation of dynamic stall for non-

stationary two-dimensional blade airfoils. In *Annual Thermofluid Conference* 4, 106–112.

Bangga, G. S. T. A., T. Lutz and E. Krämer (2015b). Numerical investigation of unsteady aerodynamic effects on thick flatback airfoils. In *Proceeding of German Wind Energy Conference 12*, Bremen, Germany 76.

Bangga, G., T. Lutz, and E. Krämer (2015a). An examination of rotational effects on large wind turbine blades. In *11th EAWE PhD Seminar*, Stuttgart, Germany.

Barakos, G. and D. Drikakis (2003). Computational study of unsteady turbulent flows around oscillating and ramping aerofoils. *International journal for numerical methods in fluids* 42(2), 163–186.

Belkheir, N., R. Dizene and S. Khelladi (2012). A numerical simulation of turbulence flow around a blade profile of HAWT rotor in moving pulse. *Journal of Applied Fluid Mechanics* 5(1), 1–9.

Chen, S. H. and C. M. Ho (1987). Near wake of an unsteady symmetric airfoil. *Journal of fluids and structures* 1(2), 151–164.

Chitsomboon, T. and C. Thamthae (2011). Adjustment of $k-\omega$ SST turbulence model for an improved prediction of stalls on wind turbine blades. In *Proceedings of the World Renewable Energy Congress* 15, 4114–4120.

Ekaterinaris, J. A. (1995). Numerical investigation of dynamic stall of an oscillating wing. *AIAA journal* 33(10), 1803–1808.

Ekaterinaris, J., G. Srinivasan and W. Mc-Croskey (1995). Present capabilities of predicting two-dimensional dynamic stall. In *AGARD Conference Proceedings*, pp. 2–2. AGARD.

Friedmann, P. (1983). Formulation and solution of rotary-wing aeroelastic stability and response problems. *Vertica* 7, 101–141.

Fung, K. Y. and L. Carr (1991). Effects of compressibility on dynamic stall. *AIAA journal* 29(2), 306–308.

Hansen, M. H., M. Gaunaa and H. Madsen (2004). *A Beddoes-Leishman type dynamic stall model in state-space and indicial formulations*. Risø National Laboratory.

Hutomo, G., G. Bangga and H. Sasongko (2016). CFD studies of the dynamic stall characteristics on a rotating airfoil. *Applied Mechanics and Materials* 836, 109–114.

Johansen, J. (1999). *Unsteady airfoil flows with application to aeroelastic stability*. Risø National Laboratory.

Johnson, W. and N. D. Ham (1972). On the mechanism of dynamic stall. *Journal of the American Helicopter Society* 17(4), 36–45.

Launder, B. E. and D. B. Spalding (1972). *Lectures in mathematical models of turbulence*.

- Academic press.
- Lee, T. and P. Gerontakos (2004). Investigation of flow over an oscillating airfoil. *Journal of Fluid Mechanics* 512, 313–341.
- Leishman, J. G. and T. Beddoes (1989). A semi-empirical model for dynamic stall. *Journal of the American Helicopter society* 34(3), 3–17.
- McCroskey, W., L. Carr and K. McAlister (1976). Dynamic stall experiments on oscillating airfoils. *Aiaa Journal* 14(1), 57–63.
- Naderi, A., M. Mojtahedpoor and A. Beiki (2016). Numerical investigation of non-stationary parameters on effective phenomena of a pitching airfoil at low Reynolds number. *Journal of Applied Fluid Mechanics* 9(2), 643–651.
- Øye, S. (1991). Dynamic stall simulated as time lag of separation. In *Proceedings of the 4th IEA Symposium on the aerodynamics of wind turbines*.
- Petot, D. (1989). Differential equation modeling of dynamic stall. *La Recherche Aerospaciale (English Edition)* 5, 59–72.
- Shih, T. H., W. W. Liou, A. Shabbir, Z. Yang and J. Zhu (1995). A new k- eddy viscosity model for high Reynolds number turbulent flows. *Computers and Fluids* 24(3), 227–238.
- Shu, C. W. (2003). High order finite difference and finite volume WENO schemes and discontinuous Galerkin methods for CFD. *International Journal of Computational Fluid Dynamics* 17(2), 107–118.
- Shur, M., P. Spalart, M. Strelets and A. Travin (1999). Detached-eddy simulation of an airfoil at high angle of attack. *Engineering turbulence modelling and experiments* 4, 669–678.
- Szydlowski, J. and M. Costes (2004). Simulation of flow around a static and oscillating in pitch naca 0015 airfoil using urans and des. In *Proceeding of ASME 2004 Heat Transfer/Fluids Engineering Summer Conference*, 891–908. American Society of Mechanical Engineers.
- Wang, S., D. B. Ingham, L. Ma, M. Pourkashanian and Z. Tao (2010). Numerical investigations on dynamic stall of low Reynolds number flow around oscillating airfoils. *Computers and Fluids* 39(9), 1529–1541.
- Wang, S., D. B. Ingham, L. Ma, M. Pourkashanian and Z. Tao (2012). Turbulence modeling of deep dynamic stall at relatively low Reynolds number. *Journal of Fluids and Structures* 33, 191–209.
- Wilcox, D. C. *et al.* (1998). *Turbulence modeling for CFD*, Volume 2. DCW industries La Canada, CA.
- Witteveen, J. A., S. Sarkar and H. Bijl (2007). Modeling physical uncertainties in dynamic stall induced fluid–structure interaction of turbine blades using arbitrary polynomial chaos. *Computers and structures* 85(11), 866–878.